Identified charged antiparticle to particle ratios near midrapidity in Cu+Cu collisions at $\sqrt{s_{NN}}$ = 62.4 and 200 GeV

B.Alver[4], B.B.Back[1], M.D.Baker[2], M.Ballintijn[4], D.S.Barton[2], R.R.Betts[6], R.Bindel[7], W.Busza[4], Z.Chai[2], V.Chetluru[6], E.García[6], T.Gburek[3], K.Gulbrandsen[4], J.Hamblen[8], I.Harnarine[6], C.Henderson[4], D.J.Hofman[6], R.S.Hollis[6], R.Hołyński[3], B.Holzman[2], A.Iordanova[6], J.L.Kane[4], P.Kulinich[4], C.M.Kuo[5], W.Li[4], W.T.Lin[5], C.Loizides[4], S.Manly[8], A.C.Mignerey[7], R.Nouicer[2], A.Olszewski[3], R.Pak[2], C.Reed[4], E.Richardson[7], C.Roland[4], G.Roland[4], J.Sagerer[6], I.Sedykh[2], C.E.Smith[6], M.A.Stankiewicz[2], P.Steinberg[2], G.S.F.Stephans[4], A.Sukhanov[2], A.Szostak[2], M.B.Tonjes[7], A.Trzupek[3], G.J.van Nieuwenhuizen[4], S.S.Vaurynovich[4], R.Verdier[4], G.I.Veres[4], P.Walters[8], E.Wenger[4], D.Willhelm[7], F.L.H.Wolfs[8], B.Wosiek[3], K.Woźniak[3], S.Wyngaardt[2], B.Wysłouch[4]

[1] Argonne National Laboratory, Argonne, IL 60439-4843, USA
[2] Brookhaven National Laboratory, Upton, NY 11973-5000, USA
[3] Institute of Nuclear Physics PAN, Kraków, Poland
[4] Massachusetts Institute of Technology, Cambridge, MA 02139-4307, USA
[5] National Central University, Chung-Li, Taiwan
[6] University of Illinois at Chicago, Chicago, IL 60607-7059, USA
[7] University of Maryland, College Park, MD 20742, USA
[8] University of Rochester, Rochester, NY 14627, USA

Antiparticle to particle ratios for identified protons, kaons and pions at $\sqrt{s_{NN}} = 62.4$ and 200 GeV in Cu+Cu collisions are presented as a function of centrality for the midrapidity region of $0.2 < \eta < 1.4$. No strong dependence on centrality is observed. For the $\langle\overline{p}\rangle/\langle p\rangle$ ratio at $\langle p_T\rangle \approx 0.51$ GeV/c, we observe an average value of $0.50 \pm 0.003_{(\mathrm{stat})} \pm 0.04_{(\mathrm{syst})}$ and $0.77 \pm 0.008_{(\mathrm{stat})} \pm 0.05_{(\mathrm{syst})}$ for the 10% most central collisions of 62.4 and 200 GeV Cu+Cu, respectively. The values for all three particle species measured at $\sqrt{s_{NN}} = 200$ GeV are in agreement within systematic uncertainties with that seen in both heavier and lighter systems measured at the same RHIC energy. This indicates that system size does not appear to play a strong role in determining the midrapidity chemical freeze-out properties affecting the antiparticle to particle ratios of the three most abundant particle species produced in these collisions.

PACS numbers: 25.75.-q, 25.75.Dw

This paper reports the first measurement of antiparticle to particle ratios of pions, kaons and protons in Cu+Cu collisions at $\sqrt{s_{NN}} = 62.4$ and 200 GeV. The data were taken during the 2005 run using the PHOBOS detector at the Relativistic Heavy Ion Collider (RHIC) at Brookhaven National Laboratory. Antiparticle to particle ratio measurements are a useful probe in the context of understanding the chemical freeze-out properties of the created state of matter. The antiproton to proton ratios, in particular, represent a direct measure of the extent to which the central collision zone is baryon free, and the data also provide additional insight into baryon transport in these collisions. A primary focus of this article is a comparison of results obtained in the Cu+Cu collision system to both smaller and larger systems in order to determine the effect of system size on the measurement.

The strength of this experimental result stems primarily from the fact that all effects of acceptance and efficiency cancel in the PHOBOS measurement of identified particle ratios. In addition, the excellent collision vertex resolution allows for a tight distance-of-closest-approach selection of identified particle tracks, which reduces contributions from weak decays and other sources of secondary particles.

Results presented here are obtained using the PHOBOS two-arm spectrometer [1]. The active elements of the tracking detectors in the spectrometer are constructed of highly segmented silicon pad sensors, with the energy deposited in each pad recorded. Each spectrometer arm has a geometrical acceptance of ± 0.1 radians in the azimuthal angle and 0.48 to 1.37 radians in polar angle ($0.2 < \eta < 1.4$). The outer 9 layers of each 15 layer spectrometer arm are located in a 2 T magnetic field provided by the dipole magnet. The magnetic field is perpendicular to the plane of the spectrometer. For a given field setting, oppositely charged particles bend in opposite directions in the plane of the spectrometer. The direction of the magnetic field is reversed frequently during the course of data taking, recording approximately the same statistics for each field setting and allowing for a dataset that further reduces systematic uncertainties arising from non-uniform beam conditions that occur in the long RHIC runs. Further details of the PHOBOS detector setup can be found in Refs. [1–3].

Due to the geometrical asymmetry of a given spectrometer arm in η-coverage, charged particles bending in opposite directions have different acceptances. Hence, to obtain the final ratios, opposite magnetic field settings for particles bending in the same direction in the same spectrometer arm are used so that they have the same acceptance. Denoting positively and negatively charged particles h^+ and h^-, at a given magnet polarity setting of

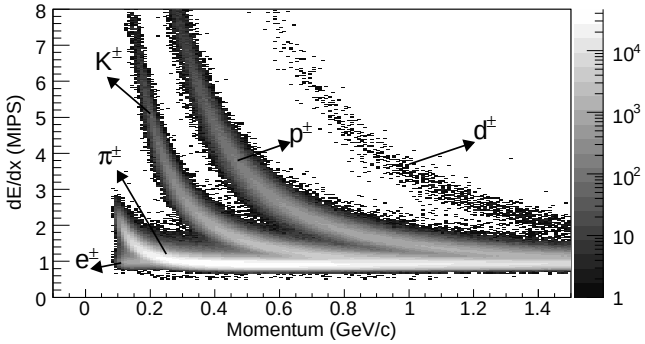

FIG. 1: Energy deposited by the reconstructed tracks in both PHOBOS spectrometer arms as a function of momentum for $\sqrt{s_{NN}}$ = 200 GeV Cu+Cu collisions. The bands are labeled for different particle species, and the current analysis is for pions, kaons and protons.

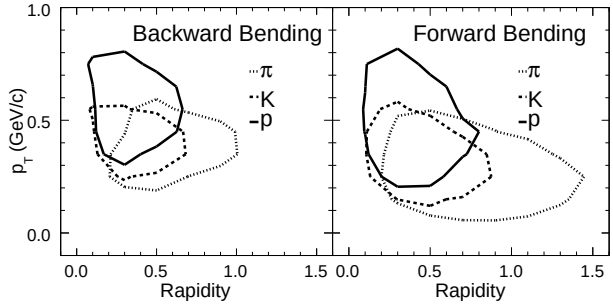

FIG. 2: Acceptance of identified particles in transverse momentum and rapidity space for $\sqrt{s_{NN}}$ = 200 GeV Cu+Cu collisions using the PHOBOS spectrometer. Backward Bending: Acceptance of particle bending away from the beam. Forward Bending: The acceptance of the particles bending towards the beam. Lines represent the 20% acceptance contour level.

B^+ or B^-, the formula for calculating the particle ratios for forward bending tracks in a given spectrometer arm for $N_{\rm h}$ particles and $N_{\rm events}$ events is

$$\frac{\langle {\rm h}^-\rangle}{\langle {\rm h}^+\rangle} = \frac{N^{\rm B^+}_{\rm h^-}(p_T, {\rm Centrality}) \times N^{\rm B^-}_{\rm events}({\rm Centrality})}{N^{\rm B^-}_{\rm h^+}(p_T, {\rm Centrality}) \times N^{\rm B^+}_{\rm events}({\rm Centrality})}.$$

In a similar manner, the formula for backward bending tracks in a given spectrometer arm is given by switching the magnet polarity setting. Four independent like-particle ratios are obtained, and the data presented are the statistically averaged results of these four measurements.

There are two steps involved in the extraction of identified particles in the spectrometer: tracking of the particles to obtain their momentum, and measurement of the energy deposited in the silicon to enable particle identification at a given momentum value. Details of the track reconstruction algorithm are described in [4]. Only particles that traversed the full spectrometer arm are included in this analysis. The track selection is based on an upper limit of 0.35 cm distance-of-closest-approach (DCA) and a χ^2 probability requirement on the tracking fit, which allows for rejection of tracks with incorrectly assigned hits and thereby improves momentum and particle identification resolution. Particle identification (PID) is based on measuring the truncated mean of the specific ionization, dE/dx, observed in the silicon detectors, as a function of momentum. The results of this are illustrated in Fig. 1 for Cu+Cu collisions at $\sqrt{s_{NN}}$ = 200 GeV. A projection of the dE/dx distribution for a given momentum bin is analyzed to produce PID bands. The choice of momentum bin size is driven by the available statistics. Local maxima are fitted with Gaussians, from which the mean and sigma are obtained as a function of momentum for each species band. Valid PID bands, versus momentum, are defined as $\pm 2\sigma$ from the mean. The upper limit of particle separation in momentum is set at the intersection of the 3σ bands, thus ensuring a negligible contamination ($< 0.1\%$). The corresponding acceptance regions for identified particles in transverse momentum, p_T, and rapidity, y, are shown in Fig. 2. As a cross-check, the PID bands were also determined using a modified Bethe-Bloch function technique, as performed in prior PHOBOS measurements [4–7]. Both approaches yield results consistent to better than 1% .

The primary hardware trigger for the Cu+Cu data was similar to that used for much of the earlier PHOBOS Au+Au data, and required at least two charged particle hits in each of the symmetrically located Paddle scintillator counters ($3.2<|\eta|<4.5$) within a time-difference of $\Delta t<10$ ns. This trigger ensures no loss of central collision events that can occur if the primary hardware trigger is based solely on the zero-degree calorimeters (ZDCs). To enhance the statistics of data near the nominal vertex position ($z_{\rm vtx} = 0$) and maximize the acceptance in the spectrometer, PHOBOS also employed two symmetrically located rings of 10 Čerenkov counters ($4.4<|\eta|<4.9$) that enabled a fast z-vertex determination.

The offline event selection utilized calibrated Paddle signals with time differences of $\Delta t \leq 5$ ns and only events with a reconstructed collision vertex of $|z_{\rm vtx}| \leq 9$ cm. The additional off-line z-vertex selection is applied to ensure good tracking efficiency and a consistent acceptance. The vertex reconstruction was optimized for the lower multiplicity Cu+Cu data through the development of two new vertex reconstruction techniques. The first technique reconstructed a high-efficiency low-resolution vertex position from the single-layered Octagon detector [8] and the second reconstructed a lower-efficiency but higher-resolution vertex position by utilizing two-hit tracklets in the Vertex detector and the first two layers of the spectrometer. A simultaneous valid vertex reconstruction in both methods was required in order to maximize data purity. This event selection is similar to that used in Ref. [9]. In addition, the data is classified into different subsets based on the run-wise $\langle x\rangle$ and $\langle y\rangle$ values of the reconstructed collision point (z-axis is parallel to the beam). As the spectrometer has a very small azimuthal acceptance, the tracking has some sensitivity to the x

and y positions of the collision. Data subsets for different polarities were matched based on this "beam orbit" classification and subsequently used for determination of the particle ratios.

The collision centrality is defined through bins of fractional total inelastic cross section, where the most central bin covering the 3% most central events is defined as 0-3%. Current results are reported down to the mid-central bin of 40-45%, with the limit set primarily by the desire for sufficient kaon statistics to enable a robust measurement. In order to divide the data into bins of fractional cross section, it is necessary to understand the trigger and vertex reconstruction efficiency of the PHOBOS detector for Cu+Cu collisions. Two methods to extract this efficiency were used to determine a total efficiency (including vertexing) of $75 \pm 5\%$ and $84 \pm 5\%$ for the 62.4 and 200 GeV Cu+Cu data, respectively. Both methods have been successfully employed for a wide range of past data covering Au+Au collisions from 19.6 to 200 GeV [10] as well as the much lower multiplicity d+Au collision data at 200 GeV [11]. It is important to note that the inefficiency is located in peripheral data and there is no inefficiency for the reported centrality bins. The data utilize the centrality classes as determined from the total energy deposited in the silicon Octagon detector [9]. The corresponding average number of participating nucleons, $\langle N_{\rm part} \rangle$, for each centrality class are calculated as detailed in Refs. [3, 9].

In order to obtain ratios of the primary yields, the inclusive (measured) particle ratios are corrected for the asymmetric absorption of antiparticles versus particles in the detector materials, contamination by secondary particles, and feed-down from hyperon decay. The methods of obtaining the correction factors, which are applied directly to the measured ratios, are similar to those used in prior analysis [6], now calculated for Cu+Cu data. The next three paragraphs summarize the techniques and magnitude of the corrections for the $\sqrt{s_{_{NN}}} = 200$ GeV data in Cu+Cu collisions. Average values for the corrections to the 62.4 GeV data are similar or smaller.

The absorption correction is obtained using a GEANT simulation of the PHOBOS beam-pipe coupled to the spectrometer acceptance. The percentage of absorbed yield is obtained for each species as a function of transverse momentum, and the final correction is obtained by taking the average of two different hadronic interaction packages, Gheisha and Fluka [12]. Proton ratios have the largest absorption correction, mainly due to increased annihilation of antiprotons as compared to protons. The absorption correction to the ratios, averaged over the accepted transverse momentum, are $\sim 1\%$, $< 0.05\%$ and $\sim 5\%$ for pions, kaons and protons, respectively.

We define secondaries as the yield of particles produced from both the beam-pipe and the PHOBOS detector material. Events from HIJING [13] are used to simulate all particles produced in the collision, which are transported using a full GEANT simulation of the detector to obtain the correction. The secondary correction to the ratios, averaged over the acceptance, is found to be $\sim 2\%$, $\sim 0\%$ and $\sim 1\%$ for pions, kaons and protons, respectively.

Feed-down particles produced from the decay of hyperons contribute to the non-primary yield, and thus must be corrected for in order to obtain the primary particle ratios. The proton ratios are more sensitive to weak decays as compared to pions and kaons [4]. The pion and kaon corrections to the individual yields essentially cancel in the final ratios, thus no correction is applied. However, the protons are more complicated. This is illustrated by the fact, known from early RHIC results, that the $\overline{\Lambda}/\Lambda$ and $\overline{p}/p$ ratios are not unity in Au+Au collisions at RHIC energies [14, 15]. Comparisons between HIJING calculations and data for protons and lambdas in Au+Au collisions have indicated differences in $\overline{\Lambda}/\overline{p}$ and Λ/p ratios of up to factors of three, with HIJING being lower than data [7]. Within PHOBOS, due to the excellent resolution of the z-vertex reconstruction ($\sigma_z \leq 0.25$ cm), a requirement of DCA less than 0.35 cm between the reconstructed tracks and event vertex is used, which removes a significant fraction of weak decays [16]. For the new Cu+Cu data, HIJING is used to obtain a baseline expectation for $\overline{\Lambda}/\overline{p}$ and Λ/p and then these ratios are varied by up to a factor of three. In addition, the calculations for Cu+Cu were manually adjusted with factors that reproduced measured values for protons and lambdas in Au+Au collisions. This work resulted in an average value used to obtain a final Λ and $\overline{\Lambda}$ feed-down correction for the proton ratios of $\sim 2.2\%$. The known variations between data and simulation for Au+Au is included in the systematic uncertainties on the proton ratio feed-down correction for Cu+Cu.

The final step in data analysis involves determination of systematic uncertainties, which arise from event selection, PID cuts, and the three correction factors. An additional contribution comes from repeating the analysis for different subsets of data based on the aforementioned $\langle x \rangle$ and $\langle y \rangle$ collision vertex position classifications. No single uncertainty (parameter) dominates the final systematic error, typically the smallest contribution comes from the PID cuts and the largest from either the event selection or, in the case of the proton ratios, the feed-down correction. The final systematic uncertainty for a given centrality is determined from the statistically weighted average of the uncertainty determined for each parameter for different arms and bending directions. A thorough investigation of the track selection χ^2 probability cut has shown a variation independent of the species and arm, but dependent on the bending direction. Hence, this effect yields a scale systematic uncertainty that, for each collision energy, is independent of both centrality and particle species.

The measured primary antiparticle to particle ratios for Cu+Cu collisions at $\sqrt{s_{_{NN}}} = 62.4$ and 200 GeV as a function of the number of participants, $N_{\rm part}$, are shown in Fig. 3. The data, also given in Tables I and II, are averaged over the acceptance as illustrated in Fig. 2. No strong centrality dependence of the proton, kaon or pion

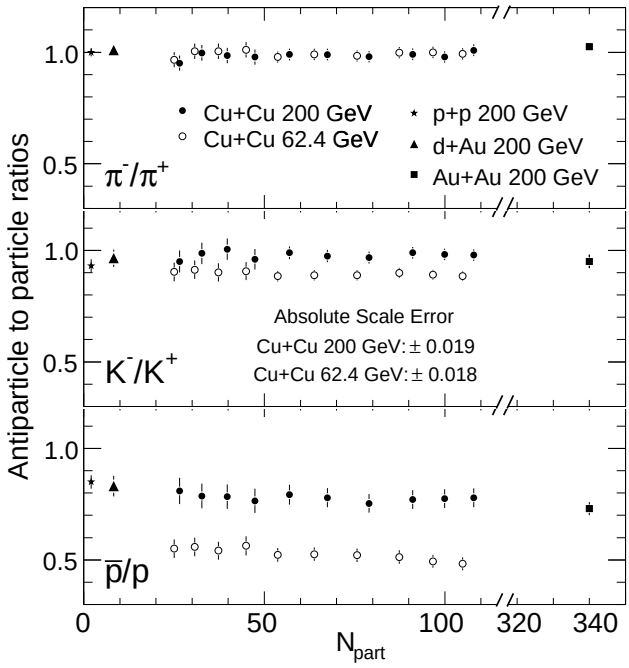

FIG. 3: Antiparticle to particle ratios in Cu+Cu collisions, as a function of the number of participants, for protons, kaons and pions. Open (closed) circles represent $\sqrt{s_{NN}} = 62.4$ GeV (200 GeV) data. The error bars represent the combined (1σ) statistical and systematic uncertainties, and an additional scale error is indicated on the figure. PHOBOS data for p+p [5], minimum-bias d+Au [6], and central Au+Au [7] collisions at $\sqrt{s_{NN}} = 200$ GeV are also shown.

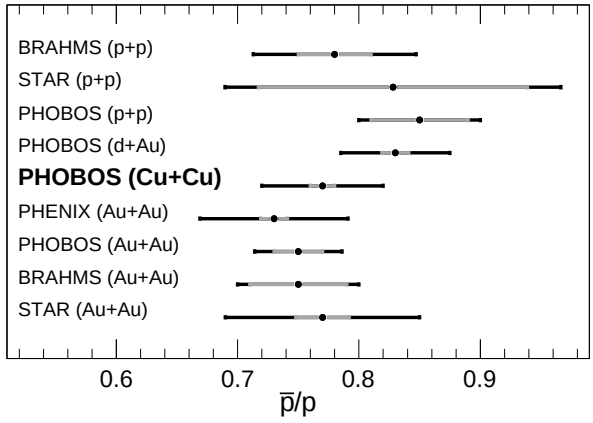

FIG. 4: Antiproton to proton ratios for $\sqrt{s_{NN}} = 200$ GeV collisions from RHIC, compared to the new result for central Cu+Cu collisions (bold). The gray bar represents the statistical error, and the black bar represents the combined statistical and systematic uncertainty. Data and references are listed in Table II.

antiparticle to particle ratios is observed. The particle ratios measured in Cu+Cu follow similar trends with collision energy as observed in Au+Au. In Cu+Cu, the pion particle ratios are consistent with unity at both 62.4 and 200 GeV, the kaon ratios have a weak collision energy dependence but reach unity at 200 GeV, and the proton ratios show the strongest variation, rising from an average value of $\langle\overline{p}\rangle/\langle p\rangle = 0.50 \pm 0.003 \pm 0.04$ at 62.4 GeV to $0.77 \pm 0.008 \pm 0.05$ at 200 GeV, for the 10% most central collisions. At the same energy of $\sqrt{s_{NN}} = 200$ GeV, the results for particle ratios of pions, kaons and protons in Cu+Cu collisions are consistent, within uncertainties, to those found by PHOBOS for p+p [5], d+Au [6] and central Au+Au [7] collisions, as shown in Fig. 3. However, the current PHOBOS data does allow for a slight decrease in the $\langle\overline{p}\rangle/\langle p\rangle$ ratio as a function of increasing $\langle N_{\rm part}\rangle$ across the different systems. Only a single minimum-bias point is shown for d+Au since, as discussed in Ref. [6], the more appropriate variable to study the centrality dependence of particle ratios in this very asymmetric system is the number of collisions per deuteron participant (ν). Similar to the present data, no centrality dependence was found in d+Au, even for the $\langle\overline{p}\rangle/\langle p\rangle$ ratio over a range of a factor of four in ν and up to a total number of participants larger than fifteen [6]. The minimum-bias point in d+Au is formed by a weighted average using combined statistical and systematic uncertainities and the associated value of $\langle N_{\rm part}\rangle = 8.3$ is given in Ref. [17].

For a more comprehensive comparison, we focus on published results of proton antiparticle to particle ratios at $\sqrt{s_{NN}} = 200$ GeV from all RHIC experiments. This compilation is shown in Figure 4 for the proton ratios, with data given in Table II. Within the current level of systematics and available data, the colliding system size appears to play only a minor role in determining the final like-particle ratios of low $\langle p_T\rangle$ pions, kaons and protons, and hence also in many of the thermal properties of the collision zone. Also, the effect of any final-state interactions on the antiparticle to particle ratios, likely present in central Cu+Cu and Au+Au collisions and absent in p+p and d+Au collisions, does not play a significant role. It is interesting to note, within the context of the present results for the intermediate Cu+Cu system, the BRAHMS Collaboration result that the strong agreement of particle ratios between the (small) p+p and (large) central Au+Au colliding systems seen at midrapidity holds out to large rapidity ($y \sim 3$), even as the ratios themselves are found to decline [18]. Table II also lists pion and kaon ratio results at RHIC, which are consistent within uncertainities.

In summary, the first results on antiparticle to particle ratios of pions, kaons and protons in Cu+Cu collisions at $\sqrt{s_{NN}} = 62.4$ and 200 GeV are reported as a function of centrality. No strong dependence on centrality is observed for the Cu+Cu data. A detailed comparison of the central Cu+Cu results at 200 GeV to results from p+p, d+Au, and central Au+Au collisions at RHIC indicates that the antiparticle to particle ratios are, for the most part, insensitive to the collision species. The final values for the antiparticle to particle ratios of pions, kaons and protons appear to be primarily driven by the collision

TABLE I: Cu+Cu collision results for antiparticle to particle ratios at $\sqrt{s_{NN}} = 62.4$ GeV. The average transverse momenta of each result is $\langle p_T \rangle \approx 0.31$, 0.36 and 0.50 GeV/c for pions, kaons and protons, respectively. The uncertainties on $\langle N_{\rm part} \rangle$ are 90% C.L. systematic and on the ratios are standard (1σ) statistical and systematic, respectively. There is an additional absolute scale systematic uncertainty of ± 0.018 on all particle ratio values. Average particle ratios, including the scale systematic uncertainty, for the 10% most central collisions are $1.00 \pm 0.001 \pm 0.03$, $0.89 \pm 0.004 \pm 0.03$ and $0.50 \pm 0.003 \pm 0.04$ for pions, kaons and protons, respectively.

Centrality	$\langle N_{\rm part} \rangle$	$\langle \pi^- \rangle / \langle \pi^+ \rangle$	$\langle K^- \rangle / \langle K^+ \rangle$	$\langle \bar{p} \rangle / \langle p \rangle$
$0-3$ %	106 ± 3	$0.99 \pm 0.002 \pm 0.03$	$0.89 \pm 0.006 \pm 0.02$	$0.48 \pm 0.005 \pm 0.03$
$3-6$ %	97 ± 3	$1.00 \pm 0.002 \pm 0.03$	$0.89 \pm 0.006 \pm 0.02$	$0.49 \pm 0.005 \pm 0.03$
$6-10$ %	88 ± 3	$1.00 \pm 0.002 \pm 0.03$	$0.90 \pm 0.007 \pm 0.02$	$0.51 \pm 0.005 \pm 0.03$
$10-15$ %	76 ± 3	$0.98 \pm 0.002 \pm 0.03$	$0.89 \pm 0.007 \pm 0.02$	$0.52 \pm 0.006 \pm 0.03$
$15-20$ %	65 ± 3	$0.99 \pm 0.002 \pm 0.03$	$0.89 \pm 0.008 \pm 0.02$	$0.53 \pm 0.006 \pm 0.03$
$20-25$ %	55 ± 3	$0.98 \pm 0.002 \pm 0.03$	$0.88 \pm 0.009 \pm 0.02$	$0.52 \pm 0.007 \pm 0.03$
$25-30$ %	47 ± 3	$1.01 \pm 0.003 \pm 0.04$	$0.91 \pm 0.011 \pm 0.04$	$0.56 \pm 0.008 \pm 0.04$
$30-35$ %	38 ± 3	$1.00 \pm 0.003 \pm 0.04$	$0.90 \pm 0.012 \pm 0.04$	$0.54 \pm 0.009 \pm 0.04$
$35-40$ %	32 ± 3	$1.00 \pm 0.003 \pm 0.04$	$0.91 \pm 0.014 \pm 0.04$	$0.56 \pm 0.010 \pm 0.04$
$40-45$ %	26 ± 3	$0.97 \pm 0.004 \pm 0.04$	$0.90 \pm 0.017 \pm 0.04$	$0.55 \pm 0.012 \pm 0.04$

TABLE II: Top: New Cu+Cu collision results for antiparticle to particle ratios at $\sqrt{s_{NN}} = 200$ GeV. The average transverse momenta of each result is $\langle p_T \rangle \approx 0.31$, 0.37 and 0.51 GeV/c for pions, kaons and protons, respectively. The given uncertainties, as well as an additional scale systematic of ± 0.019 on all Cu+Cu ratios, are as described in Table I. Bottom: Published midrapidity results for p+p, minimum-bias (minbias) d+Au and central Au+Au collisions at 200 GeV, as well as the result (including the scale systematic) for the 10% most central collisions in Cu+Cu at 200 GeV. Values are rounded to the shown precision.

Centrality	$\langle N_{\rm part} \rangle$	$\langle \pi^- \rangle / \langle \pi^+ \rangle$	$\langle K^- \rangle / \langle K^+ \rangle$	$\langle \bar{p} \rangle / \langle p \rangle$
$0-3$ %	108 ± 3	$1.01 \pm 0.003 \pm 0.03$	$0.98 \pm 0.012 \pm 0.02$	$0.78 \pm 0.013 \pm 0.04$
$3-6$ %	101 ± 3	$0.98 \pm 0.003 \pm 0.03$	$0.98 \pm 0.012 \pm 0.02$	$0.77 \pm 0.013 \pm 0.04$
$6-10$ %	91 ± 3	$0.99 \pm 0.003 \pm 0.03$	$0.99 \pm 0.013 \pm 0.02$	$0.77 \pm 0.014 \pm 0.04$
$10-15$ %	79 ± 3	$0.98 \pm 0.003 \pm 0.03$	$0.97 \pm 0.014 \pm 0.02$	$0.75 \pm 0.015 \pm 0.04$
$15-20$ %	67 ± 3	$0.99 \pm 0.003 \pm 0.03$	$0.97 \pm 0.016 \pm 0.02$	$0.78 \pm 0.016 \pm 0.04$
$20-25$ %	57 ± 3	$0.99 \pm 0.004 \pm 0.03$	$0.99 \pm 0.018 \pm 0.02$	$0.79 \pm 0.018 \pm 0.04$
$25-30$ %	48 ± 3	$0.98 \pm 0.004 \pm 0.04$	$0.96 \pm 0.019 \pm 0.04$	$0.77 \pm 0.019 \pm 0.05$
$30-35$ %	40 ± 3	$0.99 \pm 0.005 \pm 0.04$	$1.01 \pm 0.023 \pm 0.04$	$0.78 \pm 0.021 \pm 0.05$
$35-40$ %	33 ± 3	$1.00 \pm 0.005 \pm 0.04$	$0.99 \pm 0.025 \pm 0.04$	$0.79 \pm 0.024 \pm 0.05$
$40-45$ %	27 ± 3	$0.95 \pm 0.006 \pm 0.04$	$0.95 \pm 0.029 \pm 0.04$	$0.81 \pm 0.028 \pm 0.05$
Experiment (system) [Ref.]	Centrality	$\langle \pi^- \rangle / \langle \pi^+ \rangle$	$\langle K^- \rangle / \langle K^+ \rangle$	$\langle \bar{p} \rangle / \langle p \rangle$
BRAHMS (p+p) [18]	–	$1.02 \pm 0.01 \pm 0.07$	$0.97 \pm 0.05 \pm 0.07$	$0.78 \pm 0.03 \pm 0.06$
STAR (p+p) [19]	–	$0.99 \pm 0.099 \pm 0.10$	$0.94 \pm 0.111 \pm 0.09$	$0.83 \pm 0.111 \pm 0.08$
PHOBOS (p+p) [5]	–	$1.00 \pm 0.012 \pm 0.02$	$0.93 \pm 0.05 \pm 0.03$	$0.85 \pm 0.04 \pm 0.03$
PHOBOS (d+Au) [6]	minbias	$1.01 \pm 0.004 \pm 0.02$	$0.96 \pm 0.014 \pm 0.04$	$0.83 \pm 0.011 \pm 0.05$
PHOBOS (Cu+Cu)	$0-10$ %	$0.99 \pm 0.002 \pm 0.03$	$0.98 \pm 0.007 \pm 0.03$	$0.77 \pm 0.008 \pm 0.05$
PHENIX (Au+Au) [20]	$0-5$ %	$0.98 \pm 0.004 \pm 0.06$	$0.93 \pm 0.007 \pm 0.05$	$0.73 \pm 0.011 \pm 0.06$
PHOBOS (Au+Au) [7]	$0-12$ %	$1.03 \pm 0.006 \pm 0.02$	$0.95 \pm 0.03 \pm 0.03$	$0.73 \pm 0.02 \pm 0.03$
BRAHMS (Au+Au) [21]	$0-20$ %	1.00 ± 0.04	$0.95 \pm 0.05 \pm 0.04$	$0.75 \pm 0.04 \pm 0.03$
STAR (Au+Au) [22]	$0-10$ %	$1.02 \pm 0.000 \pm 0.01$	$0.97 \pm 0.026 \pm 0.10$	$0.77 \pm 0.022 \pm 0.08$

energy and, within current systematic uncertainties, are largely independent of the colliding system.

This work was partially supported by U.S. DOE grants DE-AC02-98CH10886, DE-FG02-93ER40802, DE-FG02-94ER40818, DE-FG02-94ER40865, DE-FG02-99ER41099, and DE-AC02-06CH11357, by U.S. NSF grants 9603486, 0072204, and 0245011, by Polish KBN grant 1-P03B-062-27(2004-2007), by NSC of Taiwan Contract NSC 89-2112-M-008-024, and by Hungarian OTKA grant (F 049823).

[1] B. B. Back *et al.*, Nucl. Instr. Meth. A**499**, 603 (2003).
[2] B. B. Back *et al.*, Nucl. Phys. **A661** 690, (1999).
[3] B. B. Back *et al.*, Nucl. Phys. **A757**, 28 (2005).
[4] B. B. Back *et al.*, Phys. Rev. Lett. **87**, 102301 (2001).
[5] B. B. Back *et al.*, Phys. Rev. C **71**, 021901 (2005).
[6] B. B. Back *et al.*, Phys. Rev. C **70**, 011901(R) (2004).

[7] B. B. Back *et al.*, Phys. Rev. C **67**, 021901 (2003).
[8] E. Garcia *et al.*, Nucl. Instr. Meth. A**570**, 536 (2007).
[9] B. Alver *et al.*, Phys. Rev. Lett. **96**, 212301 (2006).
[10] B. B. Back *et al.*, Phys. Rev. C **70**, 021902(R) (2004).
[11] B. B. Back *et al.*, Phys. Rev. C **72**, 031901(R) (2005).
[12] Geant Detector Simulation Tool v. 3.21, CERN.
[13] M. Gyulassy *et al.*, Phys. Rev. D **44**, 3501 (1991).
[14] K. Adcox *et al.*, Phys. Rev. Lett. **89**, 092302 (2002).
[15] C. Adler *et al.*, Phys. Rev. Lett. **86**, 4778 (2001).
[16] B. B. Back *et al.*, Phys. Rev. C **75**, 024910 (2007).
[17] B. B. Back *et al.*, Phys. Rev. C **72**, 031901 (2005).
[18] I. G. Bearden *et al.*, Phys. Lett. B **607**, 42-50 (2005).
[19] B. I. Abelev *et al.*, Phys. Rev. C **75**, 064901 (2007).
[20] S. S. Adler *et al.*, Phys. Rev. C **69**, 034909 (2004).
[21] I. G. Bearden *et al.*, Phys. Rev. Lett. **90**, 102301 (2003).
[22] G. van Buren *et al.*, Nucl. Phys. **A715**, 129c (2003).